femington

Int. J. Intell. Syst. Data Sci. (2026) 1(6):1–19
Article ID: IJISDS-2026-1050

Optimized Motion Control for Energy-Efficient Bipedal Walking Robots

Harish Kasireddy
harishkasireddy87@gmail.com
Independent Researcher

Abstract

This study explores a novel control optimization framework for bipedal robotic locomotion, focusing on energy efficiency and stability. Using a control co-design (CCD) approach, the system simultaneously optimizes mechanical parameters and control strategies to enhance gait efficiency. Within the simulation scope considered, the proposed method reduces torque demands and cycle time and yields stable walking over the simulated cycles for the reported initial conditions. Simulation results demonstrate a reduction in control effort over ten walking cycles while maintaining dynamic balance in the simulated cases, highlighting the potential of integrated design strategies in robotic walking systems.

Keywords

• Control Co-Design • Bipedal Walking Robots • Compass Gait Model • Energy-Efficient Locomotion • Trajectory Optimization • Underactuated Robotic Systems

1. Introduction

Control Co-Design (CCD) is a design method that optimally designs a system's parameters and controls the system simultaneously. Traditionally, engineering design uses an iterative process to determine the best system parameters, which can be time consuming and inefficient. It has been shown in [1] that CCD can improve the weight reduction of a high-acceleration precision motion system by 42% and its bandwidth by 28%, and [2] shows CCD can also control non-mechanical systems such as thermal management systems. Recent work has further demonstrated that data-driven control strategies, such as switched affine models, can complement CCD frameworks for building energy management [3], and machine learning approaches have been increasingly integrated with control and optimization pipelines [4].

CCD can be used with optimal control algorithms to minimize or maximize a desired cost function. One excellent resource used in this paper for both CCD and optimal control of a bipedal walking robot is Dymos [5], a multidisciplinary optimal control library that provides a platform to build and control systems with a variety of control algorithms.

In this paper, CCD is used to design the system parameters of an underactuated bipedal walking robot known as the compass gait. The limit cycle of the compass gait model and the effect of changing system parameters have been thoroughly studied in [6]. Control of the compass gait has been achieved using passive methods such as potential energy shaping [7] and active methods such as MPC control [8]; however, CCD has not been applied to the compass gait model. In this paper CCD is applied to the compass gait model using open loop control and trajectory optimization with Dymos.

© 2026 Femington Academic Publishing. All rights reserved.

The contribution of this paper is a CCD formulation for the compass gait in which the mechanical design variables (hip mass and leg-segment lengths) and the hip torque are optimized jointly over a single stride, subject to the hybrid swing-phase dynamics, the impact-transition maps, and terminal position constraints obtained from a trajectory-generation simulation. This formulation is compared against a passive compass gait and an active compass gait without co-design over ten walking cycles. The novelty relative to existing compass-gait control studies [7–9] is the joint design-and-control optimization, and the novelty relative to existing CCD studies [1, 2] is the application to an underactuated hybrid dynamical system with impact events and switching leg roles.

2. Related Work

Motion control is central to robotics and mechatronics, with foundational work integrating actuators, sensors, and controllers for advanced motion systems [10], while human motor control studies have inspired stable and efficient legged locomotion through sensory feedback and predictive control [11]. The hybrid nature of walking, combining continuous swing dynamics with discrete impact events, has motivated hybrid system models for motion control [12], complemented by control frameworks addressing actuator-level design and closed-loop performance [13].

Within legged locomotion, the compass-gait model is a canonical underactuated bipedal system for studying passive-dynamic walking, limit cycles, and stability [6, 9]. Passive methods such as potential energy shaping stabilize the compass gait [7], while active strategies including model predictive control regulate the gait [8]. Physical realizations have been built and tested experimentally, supporting the idealized model [14]. Trajectory optimization is widely used for gait generation and control, with platforms such as Dymos providing a multidisciplinary optimal-control environment [5]. These works establish the compass gait as a well-studied benchmark and provide the optimization and control foundations for the present study.

Control co-design (CCD) simultaneously optimizes physical parameters and controllers. It has improved weight reduction and bandwidth in high-acceleration precision motion systems [1] and has been applied to thermal management systems [2]. However, CCD for underactuated bipedal robots, and specifically the compass gait, remains limited: prior CCD work has focused on precision motion and thermal management rather than hybrid dynamical systems with impact events and switching leg roles. This paper addresses that gap by applying CCD to the compass gait with both passive and active optimization, formulating the co-design problem over a single optimized stride with design variables and torque optimized jointly under the hybrid dynamics and impact-transition constraints.

Beyond these core areas, data-driven and learning-based methodologies are relevant to robotic and mechatronic design and control. Machine learning has been applied to grasp synthesis for manipulation [4]; in soft robotics, data-driven dynamics and predictive optimization have been proposed for manipulators sharing the underactuated characteristics of the compass gait [15]; and decentralized control of construction vehicle fleets has been formulated as multi-agent reinforcement learning [16]. These studies show how data-driven methods complement model-based optimization in underactuated and multi-agent settings.

Machine learning has also been integrated with human-computer interaction, for example emotion recognition from EEG signals to enhance human-robot interaction [17], and frameworks bridging machine learning and human insight have been proposed for decision-making in complex systems [18], underscoring the growing importance of data-centric methodologies.

In networked systems, AI-optimized adaptive routing has been proposed for high-performance data centers [19], and orchestration of distributed deep learning atop Spark has been investigated for scalable

big data training [20], highlighting the importance of scalable computational pipelines relevant to the optimization workflows used here.

Data workflow acceleration and redundancy elimination have been addressed through smart system designs [21], and semantic synthesis of analytical pipelines has been proposed to automate workflow composition [22]. In healthcare, public sector analytics for territorial planning has used federated learning under the European Health Data Space [23], and cloud-enabled enterprise data warehouse architectures have been developed for regional health resource optimization [24]. These applications show the wide-ranging impact of data-driven methodologies sharing conceptual similarities with the optimization approaches used here.

Learning from skewed data has been addressed through modular pipelines such as ResampleCraft [25], and similar modular approaches have optimized in-database analytics for dynamic data exploration [26]. In enterprise systems, embedded intelligence for SAP S/4HANA financial close has been proposed as an automated control framework [27]. Predictive modeling has been applied to stock price direction forecasting with support vector machines [28] and to wildfire prediction and visualization [29], illustrating the diversity of domains applying optimization and control principles and reinforcing the relevance of CCD to a broad class of engineering problems.

Hybrid and evolutionary approaches have also been explored elsewhere: a hybrid method for road classification integrating aerial imagery and LiDAR [30], an evolutionary-algorithm-based AI for Tetris [31], a multi-model linguistic fusion approach for AI text generation evasion [32], and a management platform for decentralized wireless infrastructures [33]. Although outside bipedal locomotion, these share with this study a reliance on structured optimization, hybrid modeling, and system-level integration.

Compared with closely related optimization and gait-control methods, the proposed approach differs as follows. Passive control such as potential energy shaping [7] modifies the energy landscape but does not optimize mechanical design variables. Active gait control such as model predictive control [8] optimizes the control input over a prediction horizon but treats mechanical parameters as fixed. Trajectory optimization with Dymos [5] provides the transcription and optimization machinery used here, but the present study couples it with design-variable optimization in a CCD formulation. The proposed method jointly optimizes hip mass, leg-segment lengths, and hip torque under the hybrid swing-phase dynamics, the impact-transition maps, and the terminal position constraints from the trajectory-generation step. The novelty is therefore in the CCD formulation applied to the compass gait, in the use of trajectory-generation end-state constraints within that formulation, and in the single-stride open-loop co-design followed by multi-stride propagation, rather than in the individual optimization or control components.

A focused comparison summarizes this. Passive-dynamic studies [6, 9] characterize limit cycles and stability but do not optimize design variables. Energy-shaping control [7] and model predictive control [8] optimize or shape the control input with fixed mechanical parameters. CCD studies [1, 2] optimize design and control jointly but for precision motion and thermal management rather than underactuated bipedal locomotion with impact events. The present study combines CCD with the compass-gait hybrid dynamics, impact-transition maps, and trajectory-generation terminal constraints, and compares the resulting design against passive and no-co-design baselines over ten walking cycles. This supports the novelty claim while making clear that the individual components (compass-gait dynamics, Dymos transcription, CCD methodology) are established and the contribution is their specific combination in the proposed formulation.

3. Introduction to the Compass Gait

The compass gait model is an underactuated two-legged robot capable of passively walking downhill under the right initial conditions and has been extensively studied in the literature [9]. Shown in Figure 1 is a schematic showing the compass gait and its respective system parameters. The two leg masses are modeled as point masses with leg lengths a and b below and above the point mass making a total leg length l. The upper body of the robot is approximated as a point mass applied at the hip, m_H. The state variables of the system are the swing leg angle (the back leg) θ_{sw} and the stance leg (the front leg) angle θ_{st}. A torque, τ is applied at the hip to each leg in the opposite direction. The angle of the ramp which the compass gait walks on is γ.

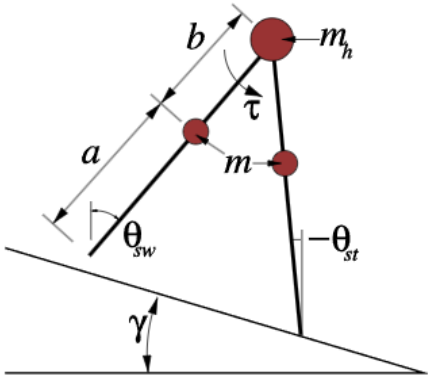


Figure 1: Schematic of the compass gait model. Angles θ_{sw} and θ_{st} are shown as the swing leg angle and stance leg angle, respectively. All geometric and dynamic quantities, including a, b, l, m, m_H, τ, and γ, are explicitly labeled.

In order to use the compass gait model a few assumptions must be made about the system. First, since the compass gait does not have the ability to bend at the hip, it must be assumed that during the swing, the swing leg retracts so that it does not collide with the ground during the swing phase. It is also assumed that a perfectly inelastic collision without sliding occurs the instant the swing leg hits the ground. The compass gait is an extremely simple model, however it should be noted that physical models of the compass gait have been built in [14].

In order to create a state space realization of the compass gait model a state matrix must be defined. For simplicity the swing and stance angles are renamed to x_1 and x_2, respectively, with x_3 and x_4 being the angular velocities of the swing and stance legs. The state vector X is shown in Eq. (1).

$$X = \begin{bmatrix} x_1 \\ x_2 \\ x_3 \\ x_4 \end{bmatrix} = \begin{bmatrix} \theta_{sw} \\ \theta_{st} \\ \dot{\theta}_{sw} \\ \dot{\theta}_{st} \end{bmatrix}, \qquad \dot{X} = \begin{bmatrix} \dot{x}_1 \\ \dot{x}_2 \\ \dot{x}_3 \\ \dot{x}_4 \end{bmatrix} = \begin{bmatrix} x_3 \\ x_4 \\ \ddot{\theta}_{sw} \\ \ddot{\theta}_{st} \end{bmatrix} = f(X, \tau). \tag{1}$$

The dynamic equations of the swing stage of the compass gait, from [6], can be written in standard planar manipulator dynamics form. This is shown in Eq. (2), where M, N, and G are the inertia, Coriolis/centrifugal, and gravity matrices defined in Appendix A, and U is the vector used to apply the torque to each leg, shown in Eq. (3).

$$M(q)\ddot{q} + N(q,\dot{q})\dot{q} + G(q) = \tau U, \qquad q = \begin{bmatrix} x_1 \\ x_2 \end{bmatrix}, \qquad \dot{q} = \begin{bmatrix} x_3 \\ x_4 \end{bmatrix}. \tag{2}$$

$$U = \begin{bmatrix} 1 \\ -1 \end{bmatrix}. \tag{3}$$

Since heel strike (when the swing leg collides with the ground) is modeled as a perfectly inelastic collision, there is an instantaneous angular velocity change when heel strike occurs. Also, since the swing leg becomes the stance leg after heel strike, the angles x_1 and x_2 must be switched in the mathematical model after each walking cycle. The transition matrices used to switch x_1 and x_2 as well as calculate the updated angular velocities after heel strike are shown in 4 and 5, where x^+ represents the state variable after heel strike and x^- represents the state variable before impact, Q^- and Q^+ are the angular velocity transition matrices shown in Appendix A.

$$\begin{bmatrix} x_1^+ \\ x_2^+ \end{bmatrix} = \begin{bmatrix} 0 & 1 \\ 1 & 0 \end{bmatrix} \begin{bmatrix} x_1^- \\ x_2^- \end{bmatrix} \tag{4}$$

$$Q^+ \begin{bmatrix} x_3^+ \\ x_4^+ \end{bmatrix} = Q^- \begin{bmatrix} x_3^- \\ x_4^- \end{bmatrix} \tag{5}$$

At each heel-strike event, the implementation applies Eq. (4) to swap the swing and stance leg angles and Eq. (5) to update the angular velocities. The pre-impact state is used to evaluate Q^- and Q^+, and the post-impact state is then used to initialize the next swing phase with the swing and stance leg roles interchanged. This switching is applied consistently at every heel-strike event in the ten-cycle simulations reported in Section 6.

4. Natural Limit Cycles of the Passive Compass Gait

It is important to define stability in the context of the compass gait for this paper. Passive control methods such as potential energy shaping have been proposed to stabilize the compass gait [7]. Active control strategies, including model predictive control, have been explored to regulate the gait [8]. Optimal control software such as Dymos provides a platform for trajectory optimization [5]. One possible meaning of stability in this context is that, while walking, the compass gait proceeds forwards in a controlled manner and takes the same "path" for each walking cycle. Or perhaps stability could be mathematically defined using Poincaré maps. While both of these definitions of stability are valid, stability in this paper simply refers to the ability of the compass gait system to continue walking forwards for the defined number of cycles. Robust control of hybrid dynamical systems provides additional theoretical background for such definitions [12].

When simulating the passive compass gait system, it can be observed that the stability of the compass gait is heavily dependent on the given initial conditions and system parameters. It can also be observed that the basin of stability is extremely small and it is almost impossible to "guess" the correct IC's and system parameters to create a stable walking system. This is one of the main issues of the compass gait, and it motivates the use of optimization and control design methods [13].

When using stable initial conditions, the compass gait can be simulated over one or multiple walking cycles. Shown in Figure 2 is an example of a stable limit cycle for the compass gait over one walking cycle. As can be seen, the swing leg makes a large arc during the swing phase of the compass gait, while

the stance leg pivots in place. The state variables during this walking cycle are also shown over time in Figure 3.

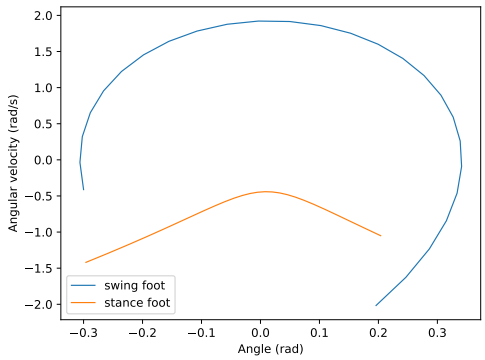


Figure 2: One walking limit cycle of the compass gait. The swing leg makes a large swing around while the stance leg only pivots.

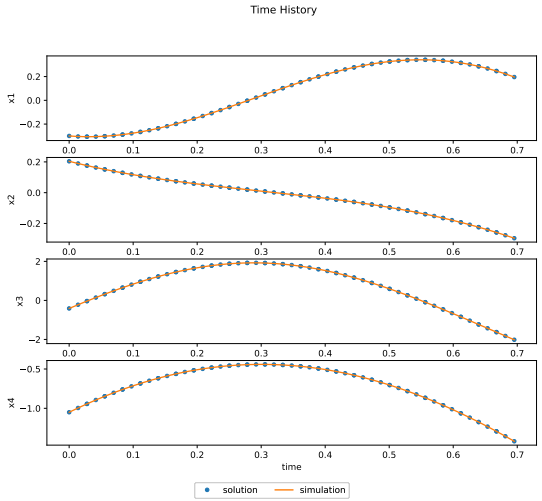


Figure 3: States of the compass gait over time for one walking cycle.

Figures 2 and 3 show the compass gait when stable initial conditions are used; however, most initial conditions given to the compass gait system result in an unstable system. An example of a unstable gait is shown in Figure 4, where the initial angular velocities are not sufficient to overcome gravity, and the compass gait cannot start a cycle and will eventually fall down. It can be seen in this figure, that the swing leg initial angle is approximately equal to the final angle of the swing leg, and the stance leg starts going forward, but runs out of momentum before falling backwards.

5. Passive Optimization with Co-Design

In order to achieve co-design with a simple passive compass gait system, an optimization problem was proposed. The CCD philosophy has been shown to improve weight reduction and bandwidth in precision motion systems [1]. It has also been applied to thermal management systems [2]. The compass gait physical models have been built and validated experimentally [14]. This optimization problem, outlined in Eq. (6), involved maximizing the point mass at the hip (m_H) in order to simulate the compass gait robot

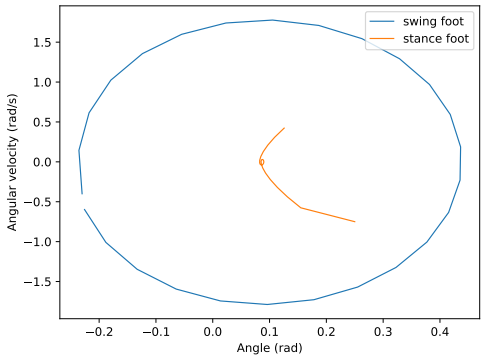


Figure 4: An example of an unstable limit cycle. In this case, the initial angular velocities make it impossible for the compass gait to start a walking cycle.

"carrying" a heavy object. In order to achieve this goal, the lengths below and above the leg point mass, a and b, were optimized. The leg point mass (m) also changed based on the total length of the legs based on the given density of the legs.

$$\begin{aligned}
&\text{Objective: Maximize } m_H \\
&\text{Subject to:} \\
&\text{Dynamic Constraints of System} \\
&\text{Design Variables: } 0.1<a<1,\ 0.1<b<1,\ (\text{m}) \\
&\text{Hip Mass: } 5<m_H<80,\ (\text{kg}) \\
&\text{Leg Mass: } m = 5(a+b),\ (\text{kg}) \\
&\text{End States } x_1 \text{ and } x_2 \text{ are Constrained Trajectory Generation}
\end{aligned} \tag{6}$$

The baseline trajectory used to generate the endpoint constraints was obtained by first simulating the passive compass-gait model from a known stable initial condition for one step and recording the terminal position states x_1 and x_2. These terminal position states were then imposed as endpoint constraints in the optimization problem. A formal sensitivity analysis with respect to different feasible initial trajectories was not performed. Because the endpoint constraints fix the terminal positions and the design variables enter nonlinearly through the dynamics, different feasible seeds may produce different local optima. This sensitivity should be examined in future work.

The goal of this optimization problem was to increase the range of initial conditions that caused the compass gait to complete one stable cycle while maximizing the mass at the hip. In order to achieve this goal a trajectory generation method was used, where the compass gait model was first simulated using known stable initial conditions and system parameters and the final position states (x_1 and x_2) were recorded and passed to the optimization model. The final position states of the optimization model were constrained to be equal to the recorded final position states found in the trajectory generation simulation. This gave the compass gait optimization problem a goal to achieve in order to keep the system stable. Figure 5 shows a diagram outlining this process.

While it was not possible to make all initial conditions stable without a controller, the range of initial conditions was increased. Shown in Figure 6 is the limit cycle of the compass gait without optimization with the initial conditions and system parameters shown in Table 1. As can be seen, the compass gait system is not able to complete a full cycle and can be said to be unstable.

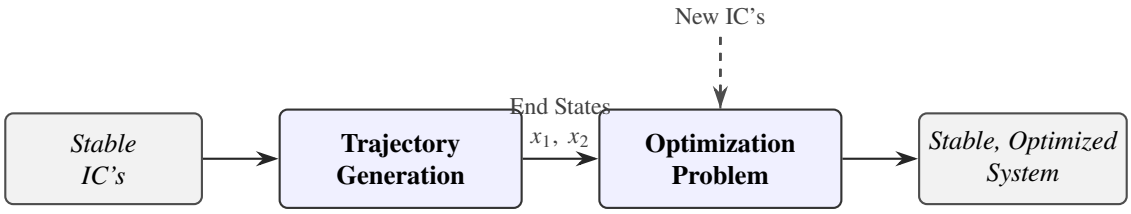


Figure 5: A trajectory generation method was used where a system with stable initial conditions found end states (x_1 and x_2) to be used for the optimization problem.

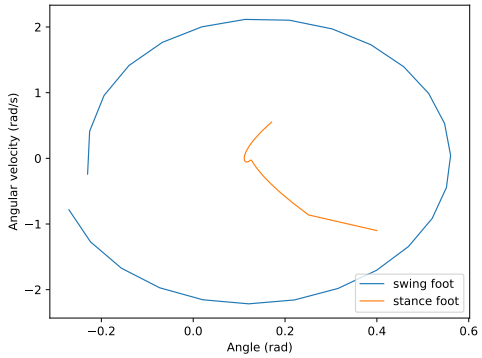


Figure 6: Limit cycle of the non optimized compass gait over one cycle with the same initial conditions as the optimized system. It can be seen that the system does not complete a full cycle.

The limit cycle of the non-optimized system can be compared to that of the optimized system in order to see the benefits of the optimization. Shown in Figure 7 is the limit cycle of the optimized compass gait system with the same initial conditions as the non-optimized compass gait. It can be seen that after optimization, the system completes a full stable walking cycle. The optimized system parameters of the new system are shown in Table 2. Not only can it be seen that the compass gait system gained stability from the optimization, but it also successfully maximized the mass at the hip. These observations are consistent with prior stability analyses of passive compass-gait limit cycles [9].

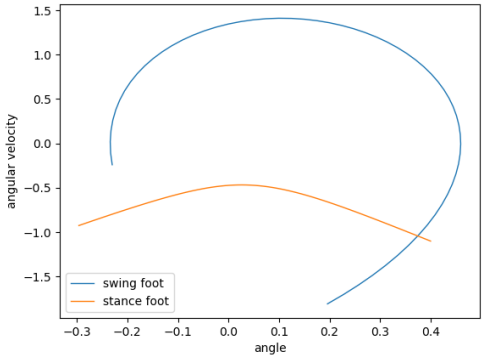


Figure 7: The limit cycle of the optimized compass gait. It can be seen that the system is stable for the first walking cycle.

While this optimization problem was successful, it has its limitations. First, as previously mentioned, without a using an active controller it is impossible to guarantee that all initial conditions for the compass gait will result in a stable walking limit cycle. Also, it is desired that the optimized compass gait system

Table 1: Initial Conditions and System Parameters of the Non-Optimized Compass Gait Shown in 6

Parameter	Value
$m(kg)$	5
$m_H(kg)$	10
$a(m)$	0.5
$b(m)$	0.5
$\gamma(slope, rad)$	0.05
$x_1(rad)$	-0.23
$x_2(rad)$	0.4
$x_3(rad/s)$	-0.24
$x_4(rad/s)$	-1.1

Table 2: Optimized System Parameters of the compass gait.

Parameter	Value
$m(kg)$	8.96
$m_H(kg)$	80
$a(m)$	0.83
$b(m)$	0.957

complete multiple walking cycles instead of just one. In order to fix these two limitations, active CCD can be used to optimize the problem and simulate the compass gait over any given number of walking cycles.

6. Active Control Co-Design of the Compass Gait

Active CCD was performed by activating a torque controller at the hip, allowing a more meaningful cost function than the passive case: the time per cycle and the total torque used were minimized. The cost function is shown in Eq. (7), where τ_r and t_r are reference scalers used to normalize τ and t, with values given in Eq. (8).

$$J = \int_0^t (\tau/\tau_r)^2 + (t/t_r)\, dt \tag{7}$$

$$\tau_r = 6.32(N * m), t_r = 0.5(s) \tag{8}$$

In Eq. (7), the integration interval is a single optimized stride, $t \in [0, t_f]$, where t_f is the stride duration. Both terms are dimensionless, so J is a dimensionless combined cost in which lower values indicate a better trade-off between control effort and cycle time.

For reproducibility: the state is $X = [x_1, x_2, x_3, x_4]^T$ from Eq. (1), the dynamics are Eq. (2) with the matrices in Appendix A, the control is the hip torque τ applied through U of Eq. (3), and heel strike uses the maps of Eq. (4) and Eq. (5). Optimization is over a single stride with terminal positions x_1, x_2 constrained to the trajectory-generation values. The design variables, bounds, leg-mass relation $m = 5(a + b)$, and cost are those of Eq. (9) and Eq. (7). The same transcription settings and node treatment are used for the CCD and no-co-design cases so that reported $\sum \tau^2$ and combined-cost values are directly comparable. Initial conditions and baseline parameters for the ten-cycle comparisons are in Table 3, and the optimized design variables are held fixed during open-loop propagation.

For Eq. (10), $\tau_{sum} = \sum_{t=0}^{t=t_f} \tau^2$ is evaluated on the Dymos collocation grid, with τ the hip torque returned by the optimizer at each node. The same node set and time-step treatment are used for the CCD and no-co-design cases, so the $\sum \tau^2$ values in Table 6 are directly comparable. Because the sum is over collocation nodes rather than a continuous integral, τ_{sum} is a discrete control-effort metric, not a physical energy in joules.

Since the hip mass was no longer in the cost function, it was also made a design variable. The constraints are given in Eq. (9).

$$
\begin{aligned}
&\text{Minimize: } J = \int_0^t (\tau/\tau_r)^2 + (t/t_r)\, dt \\
&\text{Subject to:} \\
&\text{Dynamic Constraints of System} \\
&\text{Design Variables:} \\
&0.1 < a < 1(m), 0.1 < b < 1(m), 0 < m_H < 100\text{kg} \\
&\text{Leg Mass: } m = 5(a + b) \\
&\text{End States of } x_1 \text{ and } x_2 \text{ Constrained Trajectory Generation}
\end{aligned}
\tag{9}
$$

The formulation in Eq. (9) is new in a specific sense: a, b, and m_H enter the swing dynamics through the matrices in Appendix A and the impact maps through the $Q^{\pm}$ entries, while $m = 5(a + b)$ ties geometry to both inertia and impact. The terminal positions are constrained to the trajectory-generation values, and the cost combines normalized squared torque and normalized stride time. The control strategy is open-loop torque optimization over the single stride, with design variables held fixed during the subsequent ten-cycle propagation. These elements constitute the specific new formulation relative to the passive and no-co-design baselines.

Consistent with the trajectory-generation procedure, the CCD optimization is performed over one walking cycle only, after which the optimized design variables are used in open-loop propagation over the desired number of cycles. The method is therefore single-stride open-loop co-design followed by multi-stride propagation, not full multi-cycle closed-loop co-design. Stability and robustness claims are limited to the demonstrated simulation scope: ten cycles from the initial conditions in Table 3 with fixed optimized design variables. No Poincaré-map analysis, basin-of-attraction computation, or closed-loop stability certificate is provided, and the results should not be read as a general guarantee of stable locomotion or robustness. The observed convergence to a limit cycle is a simulation-based observation, not a proof of stability.

To optimize over multiple cycles, the trajectory generation method was used with continued simulation after the first cycle: trajectory generation determines the final states, CCD optimizes the design variables and torque over one cycle, and the system is then simulated for a fixed number of cycles with torque optimization. Figure 8 outlines this process.

Three simulations were compared: active CCD (Figure 8), active open-loop control without co-design, and the non-optimized passive compass gait. Each was simulated over 10 cycles, and stability, total torque, time per cycle, and optimized design variables were compared, using the initial conditions and parameters in Table 3.

Figures 9 and 10 show the limit cycle and state time histories for the passive system. The chosen initial conditions give a stable, well-behaved response; convergence to a single limit cycle takes about three cycles, with some residual oscillation.

Figures 11 and 12 show the active open-loop control case without co-design, using the same trajectory

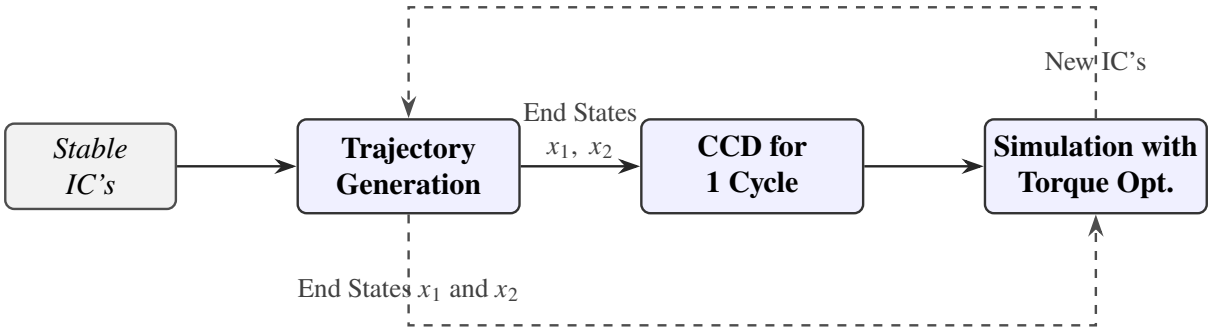


Figure 8: The trajectory generation method used in the previous example was used with continued trajectory optimization after one cycle.

Table 3: Initial Conditions and System Parameters Used to Simulate the Compass Gait.

Parameter	Value	Unit
m	5	kg
m_H	10	kg
a	0.5	m
b	0.5	m
γ	0.05	rad
x_1	-0.3	rad
x_2	0.2038	rad
x_3	-0.41215	rad/s
x_4	-1.0501	rad/s

generation method but torque optimization only. Convergence takes about six cycles, and cycles are more spaced out than in the passive system, but the final limit cycle is smaller, reducing time per cycle and total time relative to the passive system.

Figures 13 and 14 show the CCD case. One small cycle is performed before convergence to the final limit cycle in about four iterations, and time per cycle is smaller than both the passive and no-co-design systems, with much less torque than the no-co-design case.

Table 4 lists the optimized design variables. To reduce torque and time per cycle, the system prefers a higher hip mass and a longer lower leg segment; bounds should be adjusted to suit the desired design.

Table 4: Optimized Design Variables Found Using CCD.

Parameter	Value	Unit
m	6.45	kg
m_H	100	kg
a	1	m
b	0.29	m

In Table 4, $m_H = 100$ kg and $a = 1$ m are boundary solutions, indicating that the cost decreases monotonically with increasing m_H and a over the explored domain. The reported optimum is therefore conditioned on the chosen bounds and should be read as "the largest values permitted by the constraints" rather than an interior optimum. The bounds $0.1 < a < 1$ m, $0.1 < b < 1$ m, and $0 < m_H < 100$ kg keep variables physically plausible for a compass-gait-scale robot while containing the passive baseline parameters of Table 3. The upper bound $m_H = 100$ kg is unusually high and represents a stress case rather

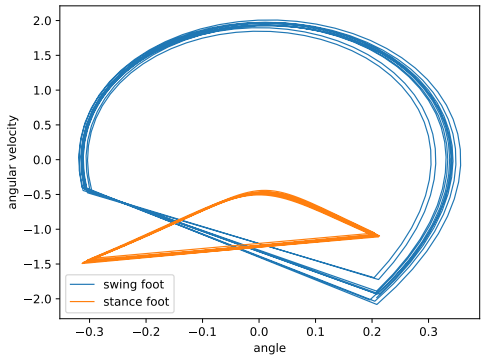


Figure 9: The limit cycle of the passive compass gait over 10 cycles.

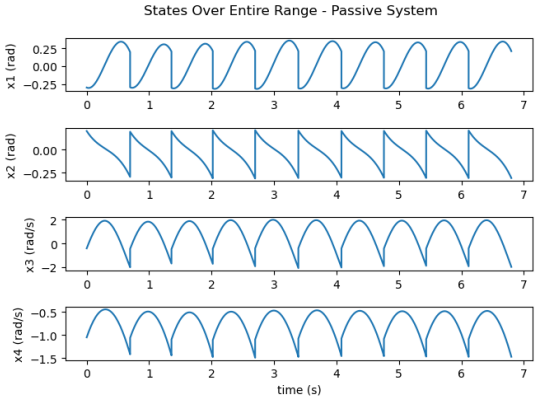


Figure 10: The total time history of the state variables of the passive compass gait over 10 cycles.

than a recommended hardware design; actuator sizing, structural loading, and walking energetics are not established here. No formal bound-sensitivity analysis was performed, so whether the improvement persists under different bounds is unknown, and these analyses are future work.

Table 5 reports average time per cycle and total time for 10 cycles. The CCD system has the shortest average time per cycle and total time, followed by open-loop control without co-design, then the passive system, so CCD is more effective at reducing cycle time than control without co-design, and any control is better than passive.

Table 5: Average Time per Cycle and Total Time for 10 Cycles of Each Simulation (in seconds)

Simulation	**Avg Time/Cycle**	**Total Time**	**% Improvement**
Passive System	0.680	6.80	N/A
Active System Without Co-Design	0.594	5.94	12.66%
System with CCD	0.531	5.31	21.91%

Table 6 compares the summation of τ^2 over all 10 cycles, defined in Eq. (10); the percent improvement is computed from the stated baseline as $(133.46 - 29.17)/133.46 \times 100\% = 78.1\%$. Much less squared torque is needed for the CCD system than for the non-optimized system. This 78.1% reduction is in a discrete control-effort metric, not in physical energy consumption, and is distinct from the 10.83% combined-objective reduction in Table 7: the combined objective also contains the normalized stride-time term, and the two systems differ in cycle time as well as torque, so the two reductions are not additive. A physically meaningful energy metric was not computed; it would require integrating mechanical power

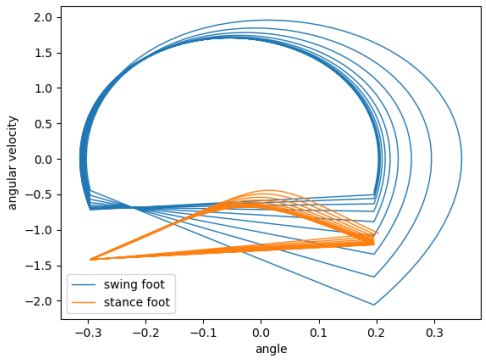


Figure 11: The limit cycle of the active compass gait using open loop control without co-design.

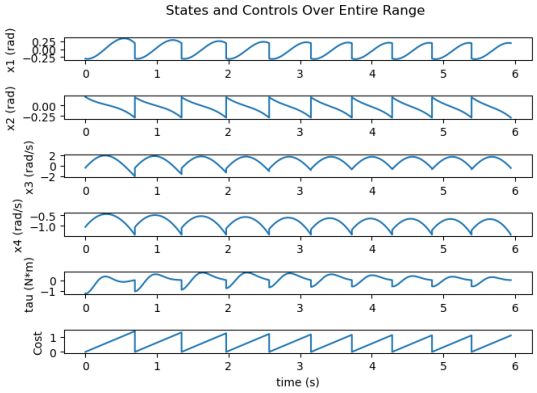


Figure 12: The total time history of the state variables, control, and cost of the active compass gait without co-design.

with explicit treatment of positive/negative work, actuator efficiency, and energy regeneration, and is identified as future work. Within the simulated cases, CCD decreases both the discrete control-effort metric and the combined cost relative to systems without co-design.

$$\tau_{sum} = \sum_{t=0}^{t=t_f} \tau^2 \tag{10}$$

Table 6: Summation of τ^2 for the CCD and Open Loop Control System

System	$\sum \tau^2$	Percent Improvement
Active System Without Co-Design	133.46	N/A
System with CCD	29.17	78.1%

7. Conclusions and Future Works

CCD was applied to the compass gait bipedal robot, first maximizing the hip mass for the passive system, then minimizing torque and time per cycle with a hip torque controller. A trajectory generation method was used in which a passive system is simulated from stable initial conditions and the end states x_1 and x_2 are used as optimization constraints to promote stability. Future work could draw on human motor

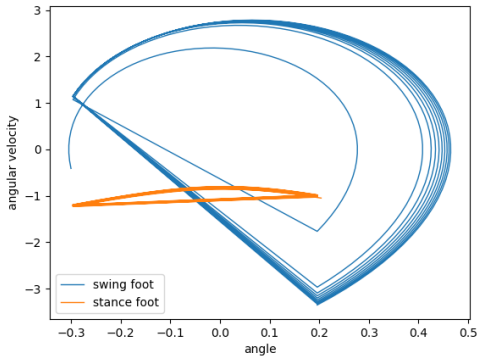


Figure 13: The limit cycle of the compass gait when CCD is used.

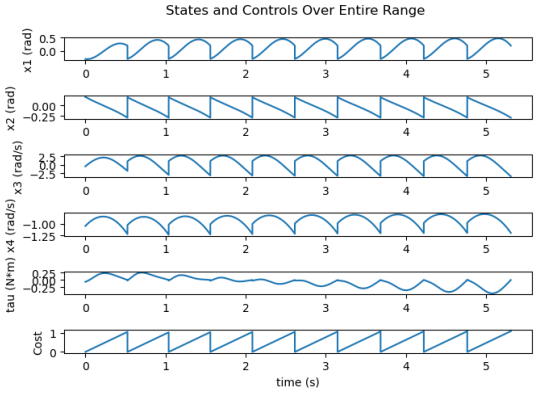


Figure 14: The total time history of the state variables, control, and cost when CCD is used.

control for gait robustness [11], advanced motion control for closed-loop CCD [10], and hybrid models for multi-cycle optimization [12].

The passive optimization showed that design-variable optimization can maximize hip mass and, for the tested initial conditions, produced a stable first walking cycle where the non-optimized system did not; this is a simulation-based observation, not a demonstration of an expanded basin of attraction.

With active CCD, the combined cost of control over 10 cycles was reduced by 10.83% relative to open-loop control without co-design under the same initial conditions and parameters. Table 7 reports the total cost over 10 cycles using the cost function of Eq. (7), with the improvement computed from the stated baseline as $(11.91 - 10.62)/11.91 \times 100\% = 10.83\%$. CCD reduced both squared torque and time per cycle: $\sum \tau^2$ fell by 78.1% (Table 6) and average time per cycle fell by 0.063 s, or 10.6%, relative to no-co-design (Table 5). These are separate metrics and are not additive; the 10.83% combined-objective reduction reflects their joint effect through Eq. (7). The 78.1% figure is a reduction in the discrete squared-torque metric of Eq. (10), not physical energy consumption. A physical energy metric was not computed and is future work.

Table 7: Cost of Control for the CCD Compass Gait vs Only Open Loop Control

System	Cost of Control
Active System Without Co-Design	11.91
System with CCD	10.62
Percent Improvement	10.83%

The ten-cycle comparisons use the single initial-condition set in Table 3 and one optimization run per configuration. A systematic robustness study across initial conditions, repeated runs from different initial guesses, and full reporting of solver convergence, computational cost, and failure cases were not performed, so the reported improvements describe the demonstrated simulation scope rather than robustness across the full initial-condition space. Sensitivity to the imposed bounds and to alternative feasible initial trajectories was not quantified. These analyses are necessary future work, and data-driven and learning-based control [15] as well as multi-agent and decentralized formulations [16] could complement such robustness studies.

A main limitation is that CCD was applied only over the first walking cycle via the trajectory generation method, after which the system was simulated with open-loop control for the given number of cycles. The results therefore correspond to single-stride open-loop co-design followed by multi-stride propagation, not full multi-cycle closed-loop co-design. The stability and performance conclusions describe only the simulated ten-cycle open-loop propagation from the initial conditions in Table 3 with fixed optimized design variables; they do not establish closed-loop stability, robustness to arbitrary initial conditions, or optimality over the full multi-cycle trajectory. Ideally, CCD for a cyclic system should optimize parameters over the entire multi-cycle trajectory; due to the structure of the Dymos code, only the first cycle could be optimized here. Future studies should optimize the compass gait over the full trajectory to obtain the best system parameters.

Beyond the single-stride limitation, experimental validation is limited in scope: three configurations (passive, active without co-design, active with CCD) over ten cycles from the single initial-condition set in Table 3. Robustness across a systematic range of initial conditions and parameters has not been established, repeated optimization runs have not been performed, and solver convergence, computational cost, and failure cases have not been reported. Sensitivity analysis for design-variable bounds and the choice of feasible initial trajectory has not been performed, and validation on a physical robot or independently validated simulator was not possible within scope. These limitations should be addressed before the improvements can be interpreted as general properties of the proposed CCD framework; in particular, additional runs with physically justified alternative bounds on m_H, a, and b are needed to test whether the improvements persist.

A further future study is closed-loop CCD, for example using MPC or LQR to optimize and control the compass gait, which would yield more optimal system parameters and better trajectory optimization.

A. Dynamics and Impact Matrices

For compactness, let

$$l = a + b, \qquad \Delta = x_2 - x_1. \tag{11}$$

The reduced coordinate vector is $q = [x_1,\ x_2]^T$, and its velocity is $\dot{q} = [x_3,\ x_4]^T$. The matrices in Eq. (2) are

$$M(q) = \begin{bmatrix} mb^2 & mlb\cos\Delta \\ mlb\cos\Delta & (m_H + m)l^2 + ma^2 \end{bmatrix}, \tag{12}$$

The inertia matrix $M(q)$ has been checked entry-by-entry against the compass-gait model of [6], using the parameter convention $l = a + b$, $\Delta = x_2 - x_1$, and the leg mass m concentrated at the point mass on each leg. The $(1, 1)$ entry mb^2 is the swing-leg inertia about the hip, the $(2, 2)$ entry $(m_H + m)l^2 + ma^2$ is the stance-leg inertia about the ground contact point including the hip mass, and the off-diagonal entries $mlb\cos\Delta$ are the corresponding inertial coupling terms. The same convention is used for the

Coriolis/centrifugal matrix N and the gravity vector G below.

$$N(q,\dot{q}) = \begin{bmatrix} 0 & -mlb\sin\Delta x_4 \\ mlb\sin\Delta x_3 & 0 \end{bmatrix}, \tag{13}$$

and

$$G(q) = \begin{bmatrix} -mbg\sin x_1 \\ -(m_H l + ml + ma)g\sin x_2 \end{bmatrix}. \tag{14}$$

The impact transition matrices Q^+ and Q^- in Eq. (5) are the standard compass-gait matrices from [6]. They have been independently checked against the cited source rather than assumed correct by virtue of being standard expressions. The heel-strike map is implemented as follows: the pre-impact state x^- is used to evaluate Q^- and Q^+, the post-impact angular velocities are obtained from Eq. (5), and the swing and stance leg angles are swapped according to Eq. (4). After the swap, the leg that was the swing leg becomes the stance leg for the next stride, and the leg that was the stance leg becomes the swing leg. This switching is applied at every heel-strike event in the simulation:

$$Q^+ = \begin{bmatrix} Q^+_{11} & Q^+_{12} \\ Q^+_{21} & Q^+_{22} \end{bmatrix}, \qquad Q^- = \begin{bmatrix} Q^-_{11} & Q^-_{12} \\ Q^-_{21} & Q^-_{22} \end{bmatrix}, \tag{15}$$

with

$$\begin{aligned} Q^+_{11} &= mb^2 + mlb\cos\Delta + mab, \\ Q^+_{12} &= mb^2 + mab, \\ Q^+_{21} &= mb^2 + mlb\cos\Delta + mab + mal\cos\Delta + ma^2, \\ Q^+_{22} &= mb^2 + mab + mal\cos\Delta + ma^2, \\ Q^-_{11} &= mb^2 + mab + mlb\cos\Delta, \\ Q^-_{12} &= mb^2 + mab, \\ Q^-_{21} &= mb^2 + mab + mlb\cos\Delta + mal\cos\Delta + ma^2, \\ Q^-_{22} &= mb^2 + mab + mal\cos\Delta + ma^2, \end{aligned} \tag{16}$$

where, as defined above, $l = a + b$ and $\Delta = x_2 - x_1$. These entries are the standard compass-gait impact-transition expressions from [6], evaluated with the same parameter convention used in Eq. (2) and the mass definitions $m = 5(a + b)$ and m_H. The equations in this appendix have been compared symbol-by-symbol with the equations implemented in the Dymos model used for the simulations. The swing-phase dynamics of Eq. (2) with the matrices M, N, and G above, the torque input vector U of Eq. (3), the angle-switching map of Eq. (4), and the velocity-transition map of Eq. (5) with the $Q^\pm$ entries above are the equations that are implemented in Dymos. No additional terms, sign conventions, or parameter definitions are used in the implementation beyond those stated in this appendix.

References

[1] Jingjie Wu and Lei Zhou. Control co-design of actively controlled lightweight structures for high-acceleration precision motion systems, 2022.

[2] Falak Mandali, Michael Shanks, and Neera Jain. Control co-design of a thermal management system with integrated latent thermal energy storage and a logic-based controller. In *2023 22nd IEEE Intersociety Conference on Thermal and Thermomechanical Phenomena in Electronic*

Systems (ITherm). IEEE, May 2023. doi: 10.1109/itherm55368.2023.10177617. URL http://dx.doi.org/10.1109/ITherm55368.2023.10177617.

[3] Dhanraj Katkar. Data-driven control for building energy management using switched affine models. In *2025 IEEE Global Conference on Wireless Computing and Networking (GCWCN)*, 2025. doi: 10.1109/GCWCN66157.2025.11448469.

[4] Tahmina Anondi. Robotics: Machine learning for data-driven grasp synthesis. In *2025 IEEE Robotics and Automation AI Conference (RAAI)*, 2025. doi: 10.1109/RAAI67517.2025.11423054.

[5] Robert Falck, Justin S. Gray, Kaushik Ponnapalli, and Ted Wright. dymos: A python package for optimal control of multidisciplinary systems. *Journal of Open Source Software*, 6(59):2809, 2021. doi: 10.21105/joss.02809. URL https://doi.org/10.21105/joss.02809.

[6] Ambarish Goswami, Benoît Thuilot, and Bernard Espiau. Compass-Like Biped Robot Part I : Stability and Bifurcation of Passive Gaits. Research Report RR-2996, INRIA, 1996. URL https://inria.hal.science/inria-00073701.

[7] M.W. Spong and G. Bhatia. Further results on control of the compass gait biped. In *Proceedings 2003 IEEE/RSJ International Conference on Intelligent Robots and Systems (IROS 2003) (Cat. No.03CH37453)*, IROS-03. IEEE. doi: 10.1109/iros.2003.1248927. URL http://dx.doi.org/10.1109/IROS.2003.1248927.

[8] A. K. Kamath and N. M. Singh. Impact dynamics based control of compass gait biped. In *2009 American Control Conference*. IEEE, 2009. doi: 10.1109/acc.2009.5160731. URL http://dx.doi.org/10.1109/ACC.2009.5160731.

[9] A. Goswami, B. Espiau, and A. Keramane. Limit cycles and their stability in a passive bipedal gait. In *Proceedings of IEEE International Conference on Robotics and Automation*, ROBOT-96. IEEE. doi: 10.1109/robot.1996.503785. URL http://dx.doi.org/10.1109/ROBOT.1996.503785.

[10] Kouhei Ohnishi, Masaaki Shibata, and Toshiyuki Murakami. Motion control for advanced mechatronics. *IEEE/ASME Transactions on Mechatronics*, 1(1):56–67, 1996. doi: 10.1109/3516.491410.

[11] David A. Rosenbaum. *Human Motor Control*. Academic Press, San Diego, CA, 2nd edition, 2009.

[12] Roger W. Brockett. Hybrid models for motion control systems. In H. L. Trentelman and J. C. Willems, editors, *Essays on Control: Perspectives in the Theory and its Applications*, volume 14 of *Progress in Systems and Control Theory*, pages 29–53. Birkhäuser Boston, Boston, MA, 1993. doi: 10.1007/978-1-4612-0317-0_2.

[13] Asif Sabanovic and Kouhei Ohnishi. *Motion Control Systems*. John Wiley & Sons, Singapore, 2011. doi: 10.1002/9780470825751.

[14] Zachary Jackowski. Design, construction, and experiments with a compass gait walking robot. 12 2011.

[15] Shubham Rahangdale. Advanced control strategy for soft robotic manipulators using data-driven dynamics and predictive optimization. Technical report, 2025.

[16] Tanish Gupta. Decentralized control of construction vehicle fleets for optimized energy consumption: A multi-agent reinforcement learning paradigm. In *IEEE*, 2025. URL https://ieeexplore.ieee.org/document/11409342.

[17] Chak Man Lam. Emotion recognition using eeg signals: Machine learning-based analysis on the mahnob-hci dataset. In *Advances in Human-Computer Interaction*. Springer, 2025. doi: 10.1007/978-3-032-19182-3_5.

[18] Aby Abraham. Bridging big data machine learning and human insight with visual interaction, 2025. URL https://ieeexplore.ieee.org/author/549808137525098. IEEE.

[19] Vishwanath Hiremath. Ai-optimized adaptive routing for high-performance data centers: A predictive framework for dynamic network optimization. In *IEEE*, 2025. URL https://ieeexplore.ieee.org/abstract/document/11211986.

[20] Priyanka Muppuri. Orchestrating distributed deep learning atop spark: A systems-centric pathway for scalable big data training. In *2025 IEEE Mediterranean Communications Conference (MEDCOM)*, 2025. doi: 10.1109/MEDCOM67532.2025.11405074.

[21] Ahmed Sarwar Mohammed. Data workflow acceleration: A smart system for redundancy elimination in machine learning pipelines. *Journal of Innovative Technology and Data Warehousing*, 2025. doi: 10.36548/jitdw.2025.4.002.

[22] Muneeb Uddin Syed. Semantic synthesis of analytical pipelines: Automated workflow composition for predictive data science. 2025. doi: 10.67231/bacg1854.

[23] Het Rachhadiya. Public sector analytics for territorial healthcare planning: Federated learning under the european health data space. 2025. doi: 10.67231/a8hswk54.

[24] Krutika Shah. Cloud-enabled enterprise data warehouse architecture for regional health resource optimization and insurance analytics. 2025. doi: 10.67231/y64edh20.

[25] Monisha Rengaraj. Resamplecraft: Modular pipelines for robust learning on skewed data. 2025. doi: 10.67231/jgme3g43.

[26] Meet Amin. Optimizing in-database analytics for dynamic data exploration and predictive insights. In *Data Analytics and Intelligent Systems*. Atlantis Press, 2025. doi: 10.2991/978-94-6239-674-6_6.

[27] Fazle Hakeem Ghory. Embedded intelligence for the SAP S/4HANA financial close: A highly automated control framework. *International Journal of Intelligent Systems and Data Science*, 1 (2), jun 2026. doi: 10.67231/s0h5b367. URL https://journals.femington.com/ijisds/article/view/447.

[28] Bhuvan Chandra Sarakam. Predicting stock price directions using support vector machines: A data science approach. In *SX Publication Conference*, 2025. URL https://www.sxpublication.co.in/conference/.

[29] N. B. Wildfire prediction and visualization: A machine learning approach using u.s. data. In *Proceedings of the International Conference on Smart Innovations in AI and Machine Learning (ICSIAIML)*. Atlantis Press, 2025. URL https://www.atlantis-press.com/proceedings/icsiaiml-25/126021208.

[30] Gangaraju Vemula. *A Hybrid Approach to Road Classification Using LiDAR Data: Integrating Aerial Imagery and Known Road Centrelines for Enhanced Feature Extraction*. PhD thesis, 2025. URL `https://zenodo.org/records/17951785`.

[31] Rayhan Khan. Development of an AI for versus tetris using evolutionary algorithms. 2025. doi: 10.67231/htp1hp30.

[32] Afsar Khan. Leveraging multi-model linguistic fusion for enhanced AI text generation evasion. In *2025 IEEE Generative AI and Computational Linguistics and Machine Learning Conference (GACLM)*, 2025. doi: 10.1109/GACLM67198.2025.11231821.

[33] Muskan Pawar. Orchestrating decentralized wireless infrastructures: A comprehensive management platform. 2025. doi: 10.67231/4z837x12.